Suppression of CO_2 outgassing by gas bubbles under a hurricane

Jun-Hong Liang[1,2,3], Eric A. D'Asaro[4], Craig L. McNeil[4], Yalin Fan[5], Ramsey R. Harcourt[4], Steve R. Emerson[6], Bo Yang[7], and Peter P. Sullivan[8]

[1] Department of Oceanography and Coastal Sciences, Louisiana State University, Baton Rouge, Louisiana, USA

[2] Center for Computation and Technology, Louisiana State University, Baton Rouge, Louisiana, USA

[3] Coastal Studies Institute, Louisiana State University, Baton Rouge, Louisiana, USA

[4] Applied Physics Laboratory, University of Washington, Seattle, Washington, USA

[5] Naval Research Laboratory, Stennis Space Center, Mississippi, USA

[6] School of Oceanography, University of Washington, Seattle, Washington, USA

[7] Department of Environmental Sciences, University of Virginia, Charlottesville, Virginia, USA

[8] National Center for Atmospheric Research, Boulder, Colorado, USA

Corresponding author: Jun-Hong Liang (jliang@lsu.edu)

Key Points:

- Gas bubbles reduce CO_2 efflux from supersaturated water by a factor of 50 under hurricane winds for the simulated conditions.
- Bubble-induced supersaturation should be included in gas flux parameterization for CO_2 in high wind conditions
- Parameterizations derived using O_2, N_2 and inert gases may not be accurate for CO_2 that has a very different solubility.

Plain Language Summary

Carbon dioxide (CO_2) is the primary anthropogenic greenhouse gases in the atmosphere and is the gas most responsible for global warming. The ocean is an important sink of anthropogenic atmospheric CO_2, yet the exchange of CO_2 between the ocean and the atmosphere is not fully understood. This study re-examines the exchange of CO_2 under hurricanes over the low-latitude ocean, using hurricane Frances (2004) as an example. Previous studies show that hurricanes significantly facilitate the outgassing of CO_2 due to the extreme wind. Those studies, however, do not explicitly consider gas bubbles. Gas bubbles, entrained into the ocean when ocean wave breaks, are ubiquitous under hurricanes also due to the extreme wind. While in the ocean, gas bubbles not only move around under the influence of the chaotic wind-driven currents and their own buoyancy, they also exchange gases with the water. Our study, using state-of-the-art computer models that concurrently simulate the chaotic ocean currents, gas bubbles, and dissolved gases, demonstrates that hurricane plays a significantly smaller role in the ocean-atmosphere transfer of CO_2 than previously estimated.

Abstract

The role of gas bubbles on the air-sea CO_2 flux during Hurricane Frances (2004) is studied using a large-eddy simulation model that couples ocean surface boundary layer turbulence, gas bubbles and dissolved gases. In the subtropical surface ocean where gases are slightly supersaturated, gases in bubbles can still dissolve due to hydrostatic pressure and surface tension exerted on bubbles. Under the simulated conditions, the CO_2 efflux with an explicit bubble effect is less than 2% of that calculated using a gas flux formula without explicit inclusion of bubble effect. The use of a gas flux parameterization without bubble-induced supersaturation contributes to uncertainty in the global carbon budget. The results highlight the importance of bubbles under high winds even for soluble gases such as CO_2 and demonstrate that gas flux parameterization derived from gases of certain solubility may not be accurate for gases of very different solubility.

1 Introduction

The transfer of carbon dioxide (CO_2) through the ocean-atmosphere interface modulates the cycling of CO_2 in the earth system and influences the amount of anthropogenic CO_2, an important greenhouse gas, absorbed in the ocean. It has now been qualitatively understood that the ocean takes in CO_2 at the high latitudes where the surface water is cold and is undersaturated in CO_2, and releases CO_2 at low latitudes where the water is warm and is supersaturated in CO_2. The quantitative estimates of ocean-atmosphere CO_2 flux, however, still contain strong uncertainties [e.g., *Wanninkhof et al.* 2009; *Woolf et al.* 2019], associated with errors in the data used to calculate CO_2 flux including gas concentrations and wind speed, and with the functional form of gas flux parameterization due to insufficient understanding of gas transfer processes particularly when the ocean is rough and gas bubbles entrained during wave breaking play a key role.

Gas bubbles alter air-sea gas exchange in two ways: First, the gas transfer rate is enhanced as gases go in and out of the ocean through bubble surfaces in addition to the sea surface. Secondly, gases still dissolve through bubbles at saturated and supersaturated water as gases in bubbles are squeezed by water pressure and surface tension; as a result, the ocean is supersaturated when the total air-sea gas flux is zero [e.g., *Woolf* 1997]. Although the enhanced gas transfer rate is already (mostly implicitly) in popular gas flux parameterizations, the bubble-induced supersaturation is thought to be unimportant for highly soluble gases such as CO_2 and is never considered in any realistic CO_2 flux calculations. A recent observational study [*Leighton et al.* 2018], however, concluded that bubble-induced supersaturation is more important than previously thought, implying that existing CO2 calculations neglecting bubble-induced supersaturation may overestimate (underestimate) efflux (influx). On the other hand, the importance of bubble-induced supersaturation for less soluble gases such as O_2 [e.g., *Vagle et al. 2010; Bushinsky* et al. 2016; *Wang et al.* 2019], inert gases [*Stanley et al.* 2009] and their ratios [e.g., *Hamme and Emerson* 2006] has already been recognized. It was also established in those studies that accurate quantification of the total air-sea gas flux requires the separation of the total gas flux into three components, viz., the gas flux through the ocean surface, that through bubbles that completely dissolved, and that through bubbles that eventually burst at the ocean surface (partially dissolved).

Since gas transfer rate increases with wind speed, it is plausible that gas transfer under hurricanes makes a significant contribution to global CO_2 flux. Based on observational data, *Bates et al.* [1998] concluded that hurricanes contribute up to half of the global CO_2 efflux. *Levy et al.* [2012] noted that the gross effect of hurricanes on CO_2 efflux is much less and is about 10% of the global CO_2 efflux because a considerable portion of the ocean under a hurricane path is undersaturated in CO_2 and vertical mixing is anomalously weak after the passage of hurricanes.

Several other studies [e.g., *Bate* 2007; *Huang and Imberger* 2010] also discuss the CO_2 efflux under hurricane conditions. While those studies debate the quantitative integral effect of hurricanes on CO_2 efflux, they all agree that strong CO_2 outgassing occurs over surface water supersaturated in CO_2 during hurricane passage due to the enhanced transfer rate associated with strong winds. Gas flux estimates in most studies implicitly include bubble-enhanced transfer rate but not bubble-induced supersaturation [e.g., *Wanninkhof* 1992; *Fairall et al.* 2011]. While parameterizations are based on gas flux measurements, including CO_2, the data for high wind are collected at high latitudes where the wind is strong but CO_2 is strongly undersaturated [e.g., *Ho et al.* 2011; *Bell et al.* 2017]. At strongly undersaturated conditions, both the gas flux through the ocean surface and that through bubbles are from the atmosphere to the ocean. It remains unknown if the gas transfer formulas derived from undersaturated water, with CO_2 influx, apply to supersaturated water, with CO_2 efflux.

The purpose of this study is to examine the effect of gas bubbles on CO_2 outgassing in supersaturated waters under Hurricane Frances (2004). The study is conducted by synthesizing in situ observations including gases and numerical solutions from a process model that simultaneously models turbulent flows, gas bubbles, and dissolved bubbles. Section 2 describes the data and the model; Section 3 presents and discusses the results; and Section 4 is a summary.

2 Data and Model Description

2.1 Data

Hurricane Frances (2004) was a category-4 hurricane in the northwestern Atlantic Ocean causing significant damage to the Bahamas and southeastern states of the U.S. A large campaign was conducted starting August 31st, 2004 to observe both sides of the air-sea interface in the path of the hurricane. Details of the field campaign, instrumentation, and available data are in *Black et al.* [2007]. For this study, the concentrations of dissolved O_2 and N_2 derived from an O_2 sensor and a gas tension device on a Lagrangian float that constantly transited across the upper 40-m or so of the ocean under the maximum hurricane winds are used (Fig. 1a) [*D'Asaro and McNeil* 2007]. Temperature and salinity from a nearby autonomous profiling Electromagnetic Autonomous Profiling Explorer (EM-APEX) float [*Sanford et al.* 2011] are also used.

2.2 Model

2.2.1 Model description

The computer solutions are obtained using the coupled-ocean-bubble-gas model [*Liang et al.* 2017]. Turbulent currents under the hurricane are simulated with the National Center for Atmospheric Research Large Eddy Simulation (NCAR-LES) model [e.g., *Sullivan and McWilliams* 2010]. The evolution of gas bubbles is tracked as Lagrangian particles and the concentration of dissolved gases are simulated using advection-diffusion equations. Model formulation and implementation are repeated in the supporting information. The next two paragraphs highlight the improvements from *Liang et al.* [2017] that are important for bubble simulations.

Bubbles are entrained into the ocean by breaking waves. In our past studies [e.g., *Liang et al.* 2017], breaking wave number density is an exponential function of breaking wave speed (c) (see equation 3.15 in *Sullivan et al.* 2007). The functional form is based on visual observation by *Melville and Matusov* [2002]. In this study, we implemented the breaking wave front distribution function ($\Lambda(c)$) from more recent infrared observations [*Zappa et al.* 2012; *Sutherland and Melville* 2013 and 2015; *Romero* 2019] that are power-law functions of c (see supporting information for details). There are more large breaking waves and less small breaking waves using the current power-law distribution function than the exponential distribution function in our previous studies (see Figure S1 in supporting information).

In addition to O_2 and N_2 that were simulated in *Liang et al.* [2017], CO_2 is also explicitly simulated in the same way as in *Liang et al.* [2011]., In the model, dissolved inorganic carbon ([DIC]=[CO_3^{2-}]+[HCO_3^{2-}]+[H_2CO_3]) and alkalinity are simulated. The partial pressure of CO_2 is diagnosed by assuming equilibrium chemistry [e.g., *Sarmiento and Gruber* 2006; *Emerson and Hedges* 2008]. Since the carbonate reaction is assumed instantaneous, our model does not have the chemical enhancement effect of CO_2 exchange that is negligible at normal ocean turbulence conditions [e.g., *Wanninkhof and Knox* 1996]. The use of equilibrium assumption in LES studies of upper ocean CO_2 is also confirmed by *Smith et al.* [2018], who compared LES simulations resolving carbonate reactions and those assuming carbonate system equilibrium and concluded that explicit consideration of carbonate reaction has minimal effect on CO_2 flux.

2.2.2 Model configuration

The model was configured in a rectangular domain of 400×400×200m with 256×256×192 grids. The simulation starts on day 245.15 (~ 3:36 AM Sept. 1st GMT) of 2004 when the dissolved gas data are available and lasts for about 1.16 days within which the wind strengthened to its maximum and weakened to about the pre-storm strength. Wind speeds at 10-m above the ocean surface (U_{10}) and sea level pressure (Fig. 1b) were interpolated from the National Oceanic and Atmospheric Administration/Hurricane Research Division (NOAA/HRD) real-time wind analysis (H*WIND) product [*Powell et al.* 1988]. The float is located on the right flank of the hurricane and the largest U_{10} over the float is greater than 52 m/s at day 0.6. Surface heat flux and freshwater flux were interpolated from the hourly NCEP Climate Forecast System Reanalysis (CFSR) product at a spatial resolution of 0.312º×0.312º [*Saha et al.* 2010]. The strong wind and precipitation also lead to strong cooling flux and freshwater flux to the ocean (Fig. 1c). Wave parameters, including Stokes drift, peak wave period, and wave energy to the ocean, are based on the solutions of wave spectrum computed using the wind-wave model WAVEWATCH III® (WWIII) [*Tolman et al.* 2009]. The WWIII model was also driven by the H*WIND product. Details about the configuration of the WWIII model were described in Fan et al. [2009]. The calculation of wave energy flux to the ocean follows *Fan and Hwang* [2017]. The waves in the front-right quadrant of the hurricane track are higher and longer due to the resonance effect caused by the movement of the storm, while those in the rear-left quadrant are lower and shorter. The atmospheric fraction of gases is constant through the simulation and is 20.9%, 78.1% and 374ppm for O_2, N_2 and CO_2, respectively. The value for atmospheric CO_2 concentration was inferred from the updated observation-based global monthly gridded sea surface CO_2 and air-sea CO_2 flux product [*Landschützer et al.* 2017].

Initial profiles of temperature, salinity, dissolved O_2 and dissolved N_2 were set based on the measurements on the floats (Figs. 2a and 2b). The initial mixed layer depth is less than 30 m. Temperature is higher and salinity is lower in the mixed layer than below, as is typical of the region [*Sanford et al.* 2011]. Dissolved N_2 is lowest in the mixed layer and increases with depth below the mixed layer. It is about 1% supersaturated in the mixed layer. Dissolved O_2 is more than 2% supersaturated in the mixed layer. In the studied region with strong surface heating and sunlight, the euphotic zone is deeper than the mixed layer, leading to higher dissolved O_2 in the thermocline than in the mixed layer. Dissolved O_2 is the largest at around 60 m, below which dissolved O_2 decreases with depth due to remineralization. Initial profiles of dissolved inorganic carbon and alkalinity (Fig. 2c) are the same as those used by *Huang and Imberger* [2010] for the same storm. The profiles are based on measurement by the R/V Knorr cruise at (22.21°N, 66.00°W) in 1997, but are increased by 9.59 mmol/kg and 4.27 mmol/kg for DIC and alkalinity, respectively, based on the observed increase in mean DIC and alkalinity in the same region and between 1997 and 2004 by *Bates* [2007].

To understand the effect of gas bubbles, two simulations were carried out, one without gas bubbles (run NB) and the other one with bubbles (run B). In the simulation without gas bubbles, the total gas flux is calculated using the parameterization by *Wanninkhof* [1992] that is commonly used in earth system models. In the parameterization, the enhanced gas transfer rate due to bubbles is implicitly included while the bubble-induced supersaturation is neglected. In the simulation with gas bubbles, gas bubbles are represented by 8 million Lagrangian particles. The total gas flux is the sum of the gas flux through bubbles and the gas flux through the ocean surface. The gas flux through bubbles is explicitly calculated from the bubble fields and the dissolved gas fields, and the gas transfer rate through the ocean surface is calculated using the formula proposed by *Goddijn-Murphy et al.* [2012] for *in situ* wind, i.e., $k_{s,660}=2.6U_{10}-5.7$.

3 Results

During the passage of the hurricane, the ocean surface cools by about two degrees. The cooling is primarily driven by the turbulent entrainment of thermocline water. Only 10% of the total cooling is caused by surface heat flux. Detailed analysis of the cold wake of the hurricane has been carried out by *D'Asaro et al.* [2007]. It plays an important role in the local atmosphere-ocean coupling [e.g., *D'Asaro et al.* 2007], and in the heat exchange between the surface and the interior oceans [*Mei et al.* 2013]. Although there is strong freshwater flux associated with precipitation during the passage of the hurricane, sea surface salinity increases (Fig 3b) due to the dominant effect of entrainment of saltier thermocline water below the mixed layer. The model captures the observed upper ocean response well, particularly during the strongest winds.

Mixed-layer dissolved O_2, dissolved N_2 and DIC all increase after the passage of the hurricane in simulations with and without gas bubbles (red lines in Figs. 3c to 3e). Similar to heat and salt, dissolved gas concentrations are controlled by air-sea surface gas flux and by entrainment of thermocline water which has different dissolved gas concentrations. Throughout the simulated period, all three gases are supersaturated with respect to their atmospheric pressure (see the comparison between the solid lines and the dashed lines in Figs. 3c, 3d and 3f), so that the surface flux is from the ocean to the atmosphere. The supersaturated condition is a combined consequence of the initial supersaturation condition, the low atmospheric pressure during the storm, the entrainment of the thermocline water immediately below the mixed layer, and the mixing of waters of different temperatures. For the three gases, the effect of entrainment dominates that of surface outgassing, and the mixed layer concentrations of gases increase.

In the simulation with bubbles, the mixed layer concentrations of all three gases increase, and are larger than in the simulation without bubbles throughout the simulated period. Given that the effect of bottom entrainment is the same for both simulations, the difference between the two simulations is from the explicit inclusion of gas bubbles. The difference between the two simulations is much more evident for O_2 and N_2 than for DIC and pCO_2. This is consistent with the conclusion in *Koch et al.* [2009] that air-sea gas flux has a minimal influence on the change of mixed-layer DIC under a hurricane and the decrease in pCO_2 is due to changes in mixed layer temperature and salinity.

To better understand the role of bubbles in air-sea gas flux, especially for CO_2 flux, the total gas flux between the ocean and the atmosphere, and the respective contribution from the two types of bubbles and the ocean surface are presented in Figs. 4a to 4c. In the simulation without bubbles, the total gas flux (black dashed lines in Figs. 4a to 4c) is from the ocean to the atmosphere for all three gases due to the supersaturation of the gases. In the simulation with bubbles, the total gas flux for both O_2 and N_2 (black solid lines in Figs. 4a and 4b) is from the atmosphere to the ocean, in the opposite direction from the surface flux (red lines) and the total flux without bubbles (black dashed lines). The gas flux through bubbles dominates the surface flux for both O_2 and N_2. The fractional contribution by completely dissolved bubbles (blue lines) is larger for N_2 than for O_2 because the solubility of N_2 is smaller than that of O_2.

With bubbles, the total gas flux of CO_2 is from the ocean to the atmosphere aside from a brief period between around day 0.58 to day 0.69 when the winds are strongest (Fig. 4c). Under the simulated conditions, the integrated CO_2 flux during the simulated period is still from the ocean to the atmosphere but is less than 2% of the flux estimated using a parameterization without explicit consideration of bubble-induced supersaturation. Except for the first 0.32 days when CO_2 is more than 8% supersaturated and U_{10}<26m/s, bubbles contribute to CO_2 dissolution although the gas is at least 3% supersaturated. In traditional gas flux parameterization without bubble-induced supersaturation, bubbles will always contribute to gas efflux in supersaturated conditions. This implies that previous studies using a traditional gas flux parameterization significantly overestimates CO_2 efflux during the passage of a hurricane. Since CO_2 is the most soluble among the three simulated gases, the relative contribution by bubbles to total gas flux is the smallest. The effect of gas bubbles becomes evident (the black and the red lines deviate) when U_{10}>30m/s. The contribution of completely dissolved bubbles is much smaller than that from partially dissolved bubbles for CO_2 that is highly soluble. This is because the fraction of gas that dissolves through partially dissolved (large) bubbles increases with increasing solubility while the fraction of a gas through completely dissolved bubbles is determined only by the atmospheric fraction of the gas.

While parameterizations for bubble-mediated gas flux including bubble-induced supersaturation have been examined for weakly soluble gases such as inert gases [*Stanley et al.* 2009], oxygen [e.g., *Atamanchuk et al.* 2020] and nitrogen [e.g., *Emerson and Bushinsky* 2016], they have never been tested with CO_2. That is likely because all CO_2 gas flux studies are conducted at high latitudes where the water is undersaturated. We compare CO_2 flux through bubbles from the LES solutions with that calculated using three parameterizations, including *Nicholson et al.* [2011], *Liang et al.* [2013]; and *Nicholson et al.* [2016] (denoted as N11, L13, and N16 hereafter). The three parameterizations explicitly include the effect of bubble-induced supersaturation that is required to predict an influx or a reduced efflux under supersaturated conditions. The parameterizations also compare well with observed concentrations of a few weakly soluble gases [e.g., *Manning et al.* 2016; *Nicholson et al.* 2016; *Liang et al.* 2017]. The three parameterizations show different prediction skill for total gas fluxes (Figs. 4d to 4f) and the gas fluxes through bubbles when compared with the LES models (Figs. 4g to 4i). Note that the three parameterizations neglect wave condition as an additional parameter. Wave condition regulates the distribution of breaking waves and boundary layer turbulence, thereby modulating both bubble entrainment [*Deike et al.* 2017] and bubble penetration [*Liang et al.* 2012]. It was shown to be important for determining gas flux [e.g., *Liang et al.* 2017] and gas transfer rate [e.g., *Brumer et al.* 2017; *Deike et al.* 2018; *Esters et al.* 2018; *Reichl and Deike* 2020].

Parameterization L13 predicts a CO_2 efflux until day 0.5 and then switches to CO_2 influx afterward. The change from efflux to influx, also in the LES solutions, is associated with the drastic decrease in pCO_2 due to the entrainment of subsurface water into the mixed layer. In parameterizations N11 and N16, the surface efflux dominates the influx through bubbles throughout the studied period. The predicted total CO_2 fluxes by the three parameterizations are all much larger in magnitude than the results from the LES model (Fig. 4f). It is likely because the equilibration time is much shorter for CO_2 than for N_2, O_2 and inert gases (see section 4b of *Woolf and Thorpe* [1991]), As a result, in many of the partially dissolved bubbles, equilibration is reached for CO_2, but not for less soluble gases such as O_2 and N_2. When generalized for CO_2, parameterizations derived from weakly soluble gases assume that equilibration is not reached for CO_2, therefore overestimating the flux through bubbles for CO_2 and other highly soluble gases.

4 Summary

This study shows that gas bubbles have a substantial effect on the transport of a soluble gas, CO_2. The outgassing of CO_2 over supersaturated water during the passage of a hurricane is smaller than previous estimates based on traditional gas flux parameterizations. The small efflux is due to gas bubbles that transfer gases into the ocean even under supersaturated conditions. At the right flank of Hurricane Frances (2004) close to the location of maximum winds, CO_2 efflux including the effect of gas bubbles is less than 2% of that calculated using a popular gas flux parameterization without bubble-induced supersaturation under the simulated conditions. These results underscore the significance of previously overlooked bubble-induced supersaturation conditions for CO_2, a highly soluble gas. They also demonstrate that parameterizations derived using weakly soluble gases such as O_2, N_2 and inert gases are not accurate for highly soluble gases such as CO_2, and vice versa.

This study focuses on changes in mixed layer dissolved gas concentration and air-sea gas flux during the passage of a hurricane. Although the CO_2 outgassing flux is substantially smaller than previous estimates, hurricanes likely still have considerable impacts on CO_2 outgassing well after their passage. As shown in Fig. 3, the mixed-layer DIC concentration after the passage of the hurricane is substantially higher than its pre-storm values due to interior mixing. Although pCO_2 is not significantly different right after the passage of the hurricane because of cooling from entrainment of thermocline water, anomalous warming over the cold wake after the hurricane [e.g., *Price et al.* 2008] increases pCO_2, leading to anomalous outgassing in the hurricane wake. On the other hand, it is also possible that the anomalously high DIC is consumed during the enhanced plankton bloom after the passage of hurricanes and is exported to the deep ocean through the sinking of organic particles. Massive ocean phytoplankton blooms after the passage of a hurricane are commonly observed [*Lin et al.* 2003; *Walker et al.* 2005; *Liu et al.* 2019]. The study of CO_2 flux over a complete hurricane wake would require a regional or a global model together with a parameterization explicitly including bubble-induced supersaturation. Our ongoing efforts are to develop a parameterization including bubble-induced supersaturation for CO_2, with both wind and wave as parameters. Future field campaign could focus on measuring CO_2 flux over supersaturated water, those measurements should include air-side fluxes and concentrations at the two sides of the ocean surface.

Acknowledgments

JHL was supported by the National Science Foundation (NSF) through grants OCE1945502 and OCE1558317. EAD, CLM and RRH were supported by NSF through grants OCE0549887, and OCE0850551 and by the Office of Naval Research through grants N00014-081-0577 and N00014-081-0575. YF was funded by the Office of Naval Research under program element 0601153N. SRE was supported by NSF through grant OCE1558476. PPS was supported by the ONR through Grant N000141410626. Computations were performed using supercomputing facilities at Louisiana State University, at the Louisiana Optical Network Initiative, and at the National Center for Atmospheric Research (NCAR). NCAR is sponsored by NSF. Data for the figures were archived at DOI:10.5281/zenodo.3975400 (https://zenodo.org/record/3975400). Computations were performed on supercomputing facilities at Louisiana State University, through the Louisiana Optical Network Infrastructure (LONI), and at the National Center for Atmospheric Research (NCAR).

References

Atamanchuk, D., J. Koelling, U. Send, & D. W. R. Wallace, (2020), Rapid transfer of oxygen to the deep ocean mediated by bubbles. *Nature Geosci.*, **13(3)**, 232-237.

Bates, N. R. (2007), Interannual variability of the oceanic CO2 sink in the subtropical gyre of the North Atlantic Ocean over the last 2 decades. *J. Geophys. Res.*, **112**, C09013, doi:10.1029/2006JC003759.

Bates, N. R., A. H. Knap, and A. F. Michaels (1998), Contribution of hurricanes to local and global estimates of air-sea exchange of CO_2, *Nature*, **395**, 58-61, doi:10.1038/25703.

Bell, T. G., Landwehr, S., Miller, S. D., Bruyn, W. J., Callaghan, A. H., Scanlon, B., et al. (2017). Estimation of bubble-mediated air–sea gas exchange from concurrent DMS and CO2 transfer velocities at intermediate–high wind speeds. *Atmospher. Chem. Phys.*, **17(14)**, 9019-9033.

Brumer, S. E., C. J. Zappa, B. W. Blomquist, C. W. Fairall, A. Cifuentes-Lorenzen, J. B. Edson, I. M. Brooks, & B. J. Huebert, (2017). Wave-Related Reynolds number parameterizations of CO_2 and DMS transfer velocities. *Geophys. Res. Lett.*, **44(19)**, 9865-9875.

Bushinsky, S. M., Emerson, S. R., Riser, S. C., & Swift, D. D. (2016). Accurate oxygen measurements on modified Argo floats using in situ air calibrations. *Limnol. Oceanogr. Methods*, **14(8)**, 491-505.

Craik, A. D. D., and S. Leibovich (1976) A rational model for Langmuir circulations, *J. Fluid Mech.*, **73**, 401-426.

D'Asaro, E. A., and C. McNeil (2007), Air-sea gas exchange at extreme winds speeds measured by autonomous oceanographic floats, *J. Mar. Res.*, **66**, 92-109.

Deane, G. B., and M. D. Stokes (2002), Scale dependence of bubble creation mechanisms in breaking waves, *Nature*, **418**, 839-844.

Deike, L., W. K. Melville, and S. Popineta (2016), Air entrainment and bubble statistics in breaking waves, *J. Fluid Mech.*, **801**, 91-129.

Deike, L., L. Lenain, & W. K. Melville, (2017). Air entrainment by breaking waves. *Geophys. Res. Lett.*, **44(8)**, 3779-3787.

Deike, L., and W. K. Melville (2018), Gas transfer by breaking waves. *Geophys. Res. Lett.*, **45(19)**, 10,482-10,492.

Emerson, S., and S. Bushinsky (2016), The role of bubbles during air-sea gas exchange, *J. Geophys. Res. Oceans*, **121**, 4360-4376.

Emerson, S. R., and J. I. Hedges (2008), *Chemical Oceanography and the Marine Carbon Cycle*, Cambridge Univ. Press, Cambridge.

Esters, L., S. Landwehr, G. Sutherland, T. G. Bell, K. H. Christensen, E. S. Saltzman, S. D. Miller, and B. Ward (2017). Parameterizing air-sea gas transfer velocity with dissipation." *J. Geophys. Res.-Oceans*, **122(4)**, 3041-3056.

Fairall, C. W., M. Yang, L. Bariteau, J. B. Edson, D. Helmig, W. McGillis, S. Pezoa, J. E. Hare, B. Huebert, and B. Blomquist (2011), Implementation of the coupled ocean-atmosphere response experiment flux algorithm with CO2, dimethyl sulfide, and O3, *J. Geophys. Res.*, 116, C00F09.

Fan, Y., I. Ginis, T. Hara, C. W. Wright, and E. J. Walsh, (2009), Numerical simulations and observations of surface wave fields under an extreme tropical cyclone. *J. Phys. Oceanogr.*, **39**, 2097-2116.

Fan, Y., and P. Hwang (2017), Kinetic energy flux budget across air-sea interface. *Ocean Modell.*, **120**, 27-40.

Fan, Y., E. Jarosz, Z. Yu, W. Rogers, T. Jensen, and J.-H. Liang (2018). Langmuir turbulence in horizontal salinity gradient. *Ocean Modell.*, **129**, 93-103.

Goddijn-Murphy, L., D. K. Woolf, and C. Marandino (2012), Space-based retrievals of air-sea gas transfer velocities using altimeters: Calibration for dimethyl sulfide, *J. Geophys. Res.*, **117**, C08028, doi:10.1029/2011JC007535.

Harcourt, R.R., (2015), An improved second-moment closure model of Langmuir turbulence. *J. Phys. Oceangr.*, **45**, 84-103.

Hamlington, P. E., L. P. V. Roekel, B. Fox-Kemper, K. Julien, and G. P. Chini (2014), Langmuir-submesoscale interactions: Descriptive analysis of multiscale frontal spin-down simulations, *J. Phys. Oceanogr.*, 44, 2249-2272.

Hamme, R., and S. Emerson (2006), Constraining bubble dynamics and mixing with dissolved gases: Implications for productivity measurements by oxygen mass balance, *J. Mar. Res.*, **64**, 73-95.

Ho, D. T., R. Wanninkhof, P. Schlosser, D. S. Ullman, D. Hebert, and K. F. Sullivan (2011), Toward a universal relationship between wind speed and gas exchange: Gas transfer velocities measured with 3He/SF6 during the Southern Ocean Gas Exchange Experiment, *J. Geophys. Res.*, 116, C00F04, doi:10.1029/2010JC006854.

Huang, P., and J. Imberger (2010), Variation of pCO2 in ocean surface water in response to the passage of a hurricane, *J. Geophys. Res.*, **115**, C10024, doi:10.1029/2010JC006185.

Keeling, R. (1993), On the role of large bubbles in air-sea gas exchange and supersaturation in the ocean. *J. Mar. Res.*, **51**, 237-271.

Koch, J., G. A. Mckinley, V. Bennington, and D. Ullman (2009), Do hurricanes cause significant interannual variability in the air-sea CO2 flux of the subtropical North Atlantic?, *Geophys. Res. Lett.*, **36**, L07606.

Kukulka, T., A. J. Plueddemann, & P.P. Sullivan, (2013), Inhibited upper ocean restratification in non-equilibrium swell conditions. *Geophys. Res. Lett.*, **40**, 3672-3676.

Lamarre, E., and W. K. Melville (1991), Air entrainment and dissipation in breaking waves, *Nature*, **351**, 469-472.

Landschützer, P., N. Gruber and D. C. E. Bakker (2017). An updated observation-based global monthly gridded sea surface pCO2 and air-sea CO2 flux product from 1982 through 2015 and its monthly climatology (NCEI Accession 0160558). Version 2.2. NOAA National Centers for Environmental Information.

Leifer, I., and R. K. Patro (2002), The bubble mechanism for methane transport from the shallow sea bed to the surface: A review and sensitivity study, *Cont. Shelf Res.*, **22**, 2409-2428.

Leighton, T. G., Coles, D. G. H., White, P. R., Srokosz, M., & Woolf, D. K. (2018). Asymmetric transfer of CO2 across a broken sea surface. *Scientific Reports*, **8(1)**. https://doi.org/10.1038/s41598-018-25818-6

Lévy, M., M. Lengaigne, L. Bopp, E. M. Vincent, G. Madec, C. Ethé, D. Kumar, and V. V. S. S. Sarma (2012), Contribution of tropical cyclones to the air-sea CO2 flux: A global view, *Global Biogeochem. Cycles*, **26**, GB2001, doi:10.1029/2011GB004145.

Liang, J.-H., J. C. McWilliams, P. P. Sullivan, and B. Baschek (2011), Modeling bubbles and dissolved gases in the ocean, *J. Geophys. Res.*, **116**, C03015, doi:10.1029/2010JC006579.

Liang, J.-H., J. C. McWilliams, P. P. Sullivan, and B. Baschek (2012), Large eddy simulation of the bubbly ocean: New insights on subsurface bubble distribution and bubble-mediated gas transfer, *J. Geophys. Res.*, **117**, C04002, doi:10.1029/2011JC007766.

Liang, J.-H., C. Deutsch, J. C. McWilliams, B. Baschek, P. P. Sullivan, and D. Chiba (2013), Parameterizing bubble-mediated air-sea gas exchange and its effect on ocean ventilation, *Global Biogeochem. Cycles*, **27**, 894-905, doi:10.1002/gbc.20080.

Liang, J.-H., S. R. Emerson, E. A. D'Asaro, C. L. McNeil, R. R. Harcourt, P. P. Sullivan, B. Yang, and M. F. Cronin (2017), On the role of sea-state in bubble-mediated air-sea gas flux during a winter storm. *J. Geophys. Res. Oceans*, **122**, 2671-2685, https://doi.org/10.1002/2016JC012408.

Liang, J.-H., Wan, X., Rose, K. A., Sullivan, P. P., & McWilliams, J. C. (2018). Horizontal dispersion of buoyant materials in the ocean surface boundary layer. *J. Phys. Oceanogr.*, **48**, 2103-2125.

Lin, I.-I., W. T. Liu, C. C. Wu, G. T. Wong, C. Hu, Z. Chen, et al. (2003). New evidence for enhanced ocean primary production triggered by tropical cyclone. *Geophys. Res. Lett.*, **30(13)**, 1718.

Liu, B., E. J. D'Sa, and I. D. Joshi (2019). Floodwater impact on Galveston Bay phytoplankton taxonomy, pigment composition and photo-physiological state following Hurricane Harvey from field and ocean color (Sentinel-3A OLCI) observations. *Biogeosciences*, **16(9)**, 1975-2001.

Liu, J., J.-H. Liang, J. C. McWilliams, P. P. Sullivan, Y. Fan, & Q. Chen, (2018). Effect of planetary rotation on oceanic surface boundary layer turbulence. *J. Phys. Oceanogr.*, **48**, 2057-2080.

Manning, C. C., R. H. R. Stanley, D. P. Nicholson, and M. E. Squibb (2016), Quantifying air-sea gas exchange using noble gases in a coastal upwelling zone, *IOP Conf. Ser. Earth Environ. Sci.*, **35**, 012017, doi:10.1088/1755-1315/35/1/012017.

McWilliams, J. C., P. P. Sullivan, C. H. Moeng (1997), Langmuir turbulence in the ocean, *J. Fluid Mech.*, **334**, 1-30.

Mei, W., F. Primeau, J. C. McWilliams, and C. Pasquero, 2013: Sea surface height evidence for long-term warming effects of tropical cyclones on the ocean. *Proc. Natl. Acad. Sci. USA*, **110**, 15,207-15,210.

Melville, W. K., and P. Matusov (2002), Distribution of breaking waves at the ocean surface, *Nature*, **417**, 58-63.

Melville, W. K., F. Verron, and C. J. White (2002), The velocity field under breaking waves: Coherent structures and turbulence, *J. Fluid Mech.*, **454**, 203-233

McNeil, C., and E. D'Asaro (2007), Parameterization of air-sea gas fluxes at extreme wind speeds, *J. Mar. Syst.*, **66**, 110–121.

Nicholson, D. P., S. R. Emerson, S. Khatiwala, and R. C. Hamme (2011), An inverse approach to estimate bubble-mediated air-sea gas flux from inert gas measurements, paper presented at 6th *International Symposium on Gas Transfer at Water Surfaces*, Kyoto Univ. Press, pp. 223-237.

Nicholson, D. P., S. Khatiwala, and P. Heimbach (2016), Noble gas tracers of ventilation during deep-water formation in the Weddell Sea, *IOP Conf. Ser. Earth Environ. Sci.*, **35(1)**, 012019, doi:10.1088/1755-1315/35/1/012019.

Polton, J. A., D. M. Lewis, and S. E. Belcher (2005), The role of wave-induced Coriolis-Stokes forcing on the wind-driven mixed layer. *J. Phys. Oceanogr.*, **35**, 444-457.

Rabe, T. J., T. Kukulka, I. Ginnis, T. Hara, B. Reichl, E. D'Asaro, R. Harcourt & P. P. Sullivan, (2015) Langmuir turbulence under Hurricane Gustav. *J. Phys. Oceanogr.*, **45**, 657-677.

Reichl, B. G., and L. Deike (2020). Contribution of sea-state dependent bubbles to air-sea carbon dioxide fluxes. *Geophys. Res. Lett.*, e2020GL087267.

Romero, L. (2019), Distribution of surface wave breaking fronts. *Geophys. Res. Lett.*, **46**, 10463-10474.

Saha, S., Moorthi, S., Pan, H.-L., Wu, X., Wang, J., Nadiga, S., et al. (2010). The NCEP Climate Forecast System Reanalysis. *Bull. Am. Meteorol. Soc.*, **91(8)**, 1015-1058.

Sanford, T. B., J. F. Price, and J. B. Girton (2011), Upper ocean response to Hurricane Frances (2004) observed by profiling EM-APEX floats, *J. Phys. Oceanogr.*, **41**, 1041-1056, doi:10.1175/2010JPO4313.1.

Sarmiento, J. L., and N. Gruber (2006), *Ocean Biogeochemical Dynamics*, Princeton Univ. Press, Princeton, N. J.

Smith, K. M., P. E. Hamlington, K. E. Niemeyer, B. Fox-Kemper, and N. S. Lovenduski (2018), Effects of Langmuir turbulence on upper ocean carbonate chemistry. *J. Adv. Model. Earth Syst.*, **10(12)**, 3030-3048.

Stanley, R. H. R., W. J. Jenkins, D. E. Lott III, and S. C. Doney (2009), Noble gas constraints on air-sea gas exchange and bubble fluxes, *J. Geophys. Res.*, **114**, C11020, doi:10.1029/2009JC005396.

Sullivan, P. P., and J. C. McWilliams (2010), Dynamics of winds and currents coupled to surface waves, *Annu. Rev. Fluid Mech.*, **42**, 19-42, doi:10.1146/annurev-fluid-121108-145541.

Sullivan, P. P., J. C. McWilliams, and W. K. Melville (2007), Surface gravity wave effects in the oceanic boundary layer: Large eddy simulation with vortex force and stochastic breakers, *J. Fluid Mech.*, **593**, 405-452.

Sullivan, P. P. and E. G. Patton (2011), The effect of mesh resolution on convective boundary layer statistics and structures generated by large-eddy simulation. *J. Atmos. Sci.*, **68**, 2395-2415.

Sullivan, P. P., L. Romero, J. C. McWilliams, and W. K. Melville (2012), Transient evolution of Langmuir turbulence in ocean boundary layers driven by hurricane winds and waves. *J. Phys. Oceanogr.*, **42**, 1959-1980.

Sutherland, P., and W. K. Melville (2013), Field measurements and scaling of ocean surface wave-breaking statistics, Geophys. Res. Lett., **40**, 3074–3079, doi:10.1002/grl.50584.

Sutherland, P., and W. K. Melville (2015), Field measurements of surface and near-surface turbulence in the presence of breaking waves. *J. Phys. Oceanogr.*, **45**, 943-965.

Suzuki, N., and B. Fox-Kemper (2016), Understanding Stokes forces in the wave-averaged equations, *J. Geophys. Res. Oceans*, **121**, 3579-3596, doi:10.1002/2015JC011566.

Tolman, H. L., (2009). User manual and system documentation of WAVEWATCH-III version 3.14. NOAA/NWS/NCEP/MMAB Tech. Rep. 276, 220 pp.

Vagle, S., C. McNeil, and N. Steiner (2010), Upper ocean bubble measurements from the NE pacific and estimates of their role in air-sea gas transfer of the weakly soluble gases nitrogen and oxygen, *J. Geophys. Res.*, **115**, C12054.

Van Roekel, L. P., B. Fox-Kemper, P. P. Sullivan, P. E. Hamlington, and S. R. Haney (2012), The form and orientation of Langmuir cells for misaligned winds and waves, *J. Geophys. Res.*, 117, C05001, doi:10.1029/2011JC007516.

Walker, N., R. R. Leben, and S. Balasubramanian, (2005), Hurricane forced upwelling and chlorophyll-a enhancement within cold core cyclones in the Gulf of Mexico. *Geophys. Res. Lett.*, **32**, L18610, doi:10.1029/2005GL023716.

Wang, C., R. Pawlowicz, & A. R. Sastri, (2019), Diurnal and seasonal variability of near-surface oxygen in the Strait of Georgia. *J. Geophys. Res.-Oceans*, **124**, 2418-2439.

Wanninkhof, R. (1992), Relationship between wind speed and gas exchange over the ocean, *J. Geophys. Res.*, **97(C5)**, 7373–7382, doi: 10.1029/92JC00188.

Wanninkhof, R., and M. Knox (1996), Chemical enhancement of CO2 exchange in natural waters, *Limnol. Oceanogr.*, **41**, 689-698.

Wanninkhof, R., W. E. Asher, D. T. Ho, C. Sweeney, and W. R. McGillis (2009), Advances in quantifying air-sea gas exchange and environmental forcing, *Annu. Rev. Mar. Sci.*, **1**, 213-244.

Wilson, J. D. (2015), Computing the flux footprint, *Boundary-Layer Meteorol.*, **156**, 1-14.

Woolf, D. K. (1997), Bubbles and their role in gas exchange, in *The Sea Surface and Global Change*, edited by P. S. Liss and R. A. Duce, pp. 173–205, Cambridge Univ. Press, Cambridge.

Woolf, D. K., Shutler, J. D., Goddijn-Murphy, L., Watson, A. J., Chapron, B., Nightingale, P. D., et al. (2019). Key uncertainties in the recent air-sea flux of CO2. *Global Biogeochem. Cycles*, **33**, 1548-1563.

Woolf, D. K., and S. A. Thorpe (1991), Bubbles and the air-sea exchange of gases in near-saturation conditions, *J. Mar. Res.*, **49**, 435-466.

Zappa, C. J., M. L. Banner, H. Schultz, J. R. Gemmrich, R. P. Morison, D. A. LeBel, and T. Dickey (2012), An overview of sea state conditions and air-sea fluxes during RaDyO, *J. Geophys. Res.*, **117**, C00H19.

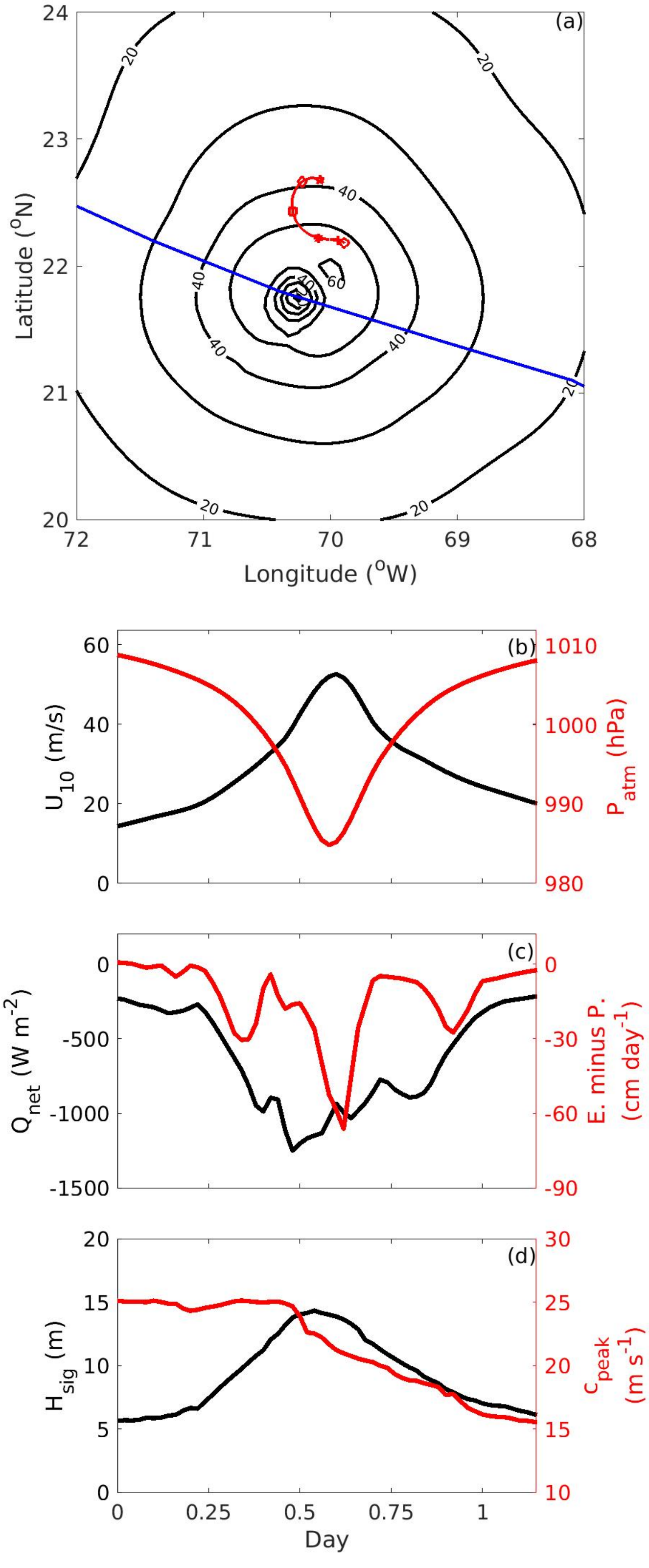

(a)
Latitude (°N)
Longitude (°W)
24
23
22
21
20
72
71
70
69
68
20
40
60
(b)
U10 (m/s)
Patm (hPa)
60
40
20
0
1010
1000
990
980
(c)
Qnet (W m-2)
E. minus P. (cm day-1)
0
-500
-1000
-1500
-30
-60
-90
(d)
Hsig (m)
cpeak (m s-1)
15
10
5
30
25
20
Day
0.25
0.5
0.75
1

517

Figure 1. (a) Contours of wind speed [m/s] for Hurricane Frances (2004) at day 245.75. The blue line is the track of the hurricane. The red line is the path of the float where measurement is taken, with symbols indicating a quarter-day increment. At the location of the float, (b) 10-m wind speed (U_{10}) and sea level pressure (P_{atm}). (c) Surface heat flux (Q_{net}) and evaporation minus precipitation (E.minusP.). (d) Significant wave height (H_{sig}) and peak wave speed (c_{peak}). Time 0 corresponds to day 245.15 of year 2004.

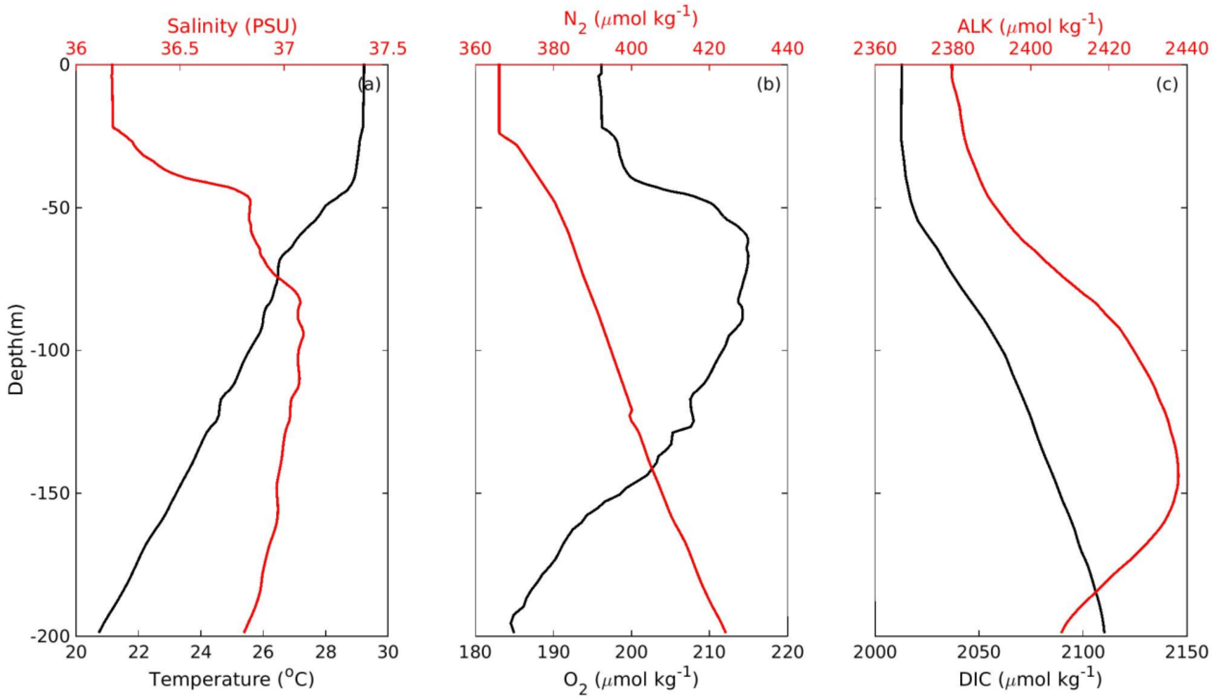

Figure 2. Initial profiles of (a) temperature and salinity; (b) dissolved O_2 and N_2; and (c) DIC and alkalinity.

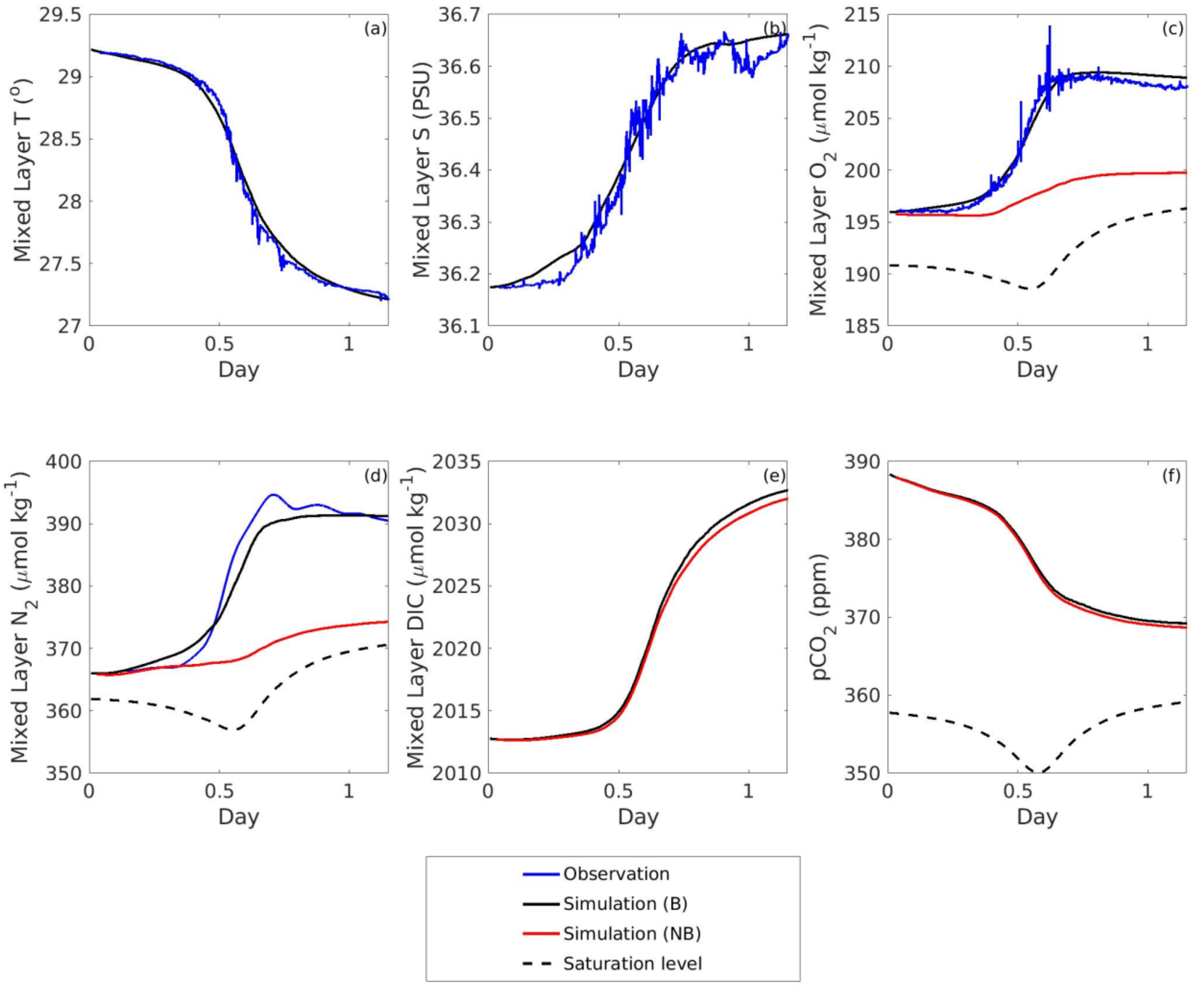

Figure 3. The evolution of simulated and observed mixed-layer (a) temperature; (b) salinity; (c) dissolved O_2 concentration; (d) dissolved N_2 concentration; (e) DIC; and (f) pCO2. Blue lines are from observation; black lines are from simulation with bubbles; red lines are from simulation without bubbles; and dashed lines are the saturation levels. The black line and the blue line overlaps in panels (a) and (b).

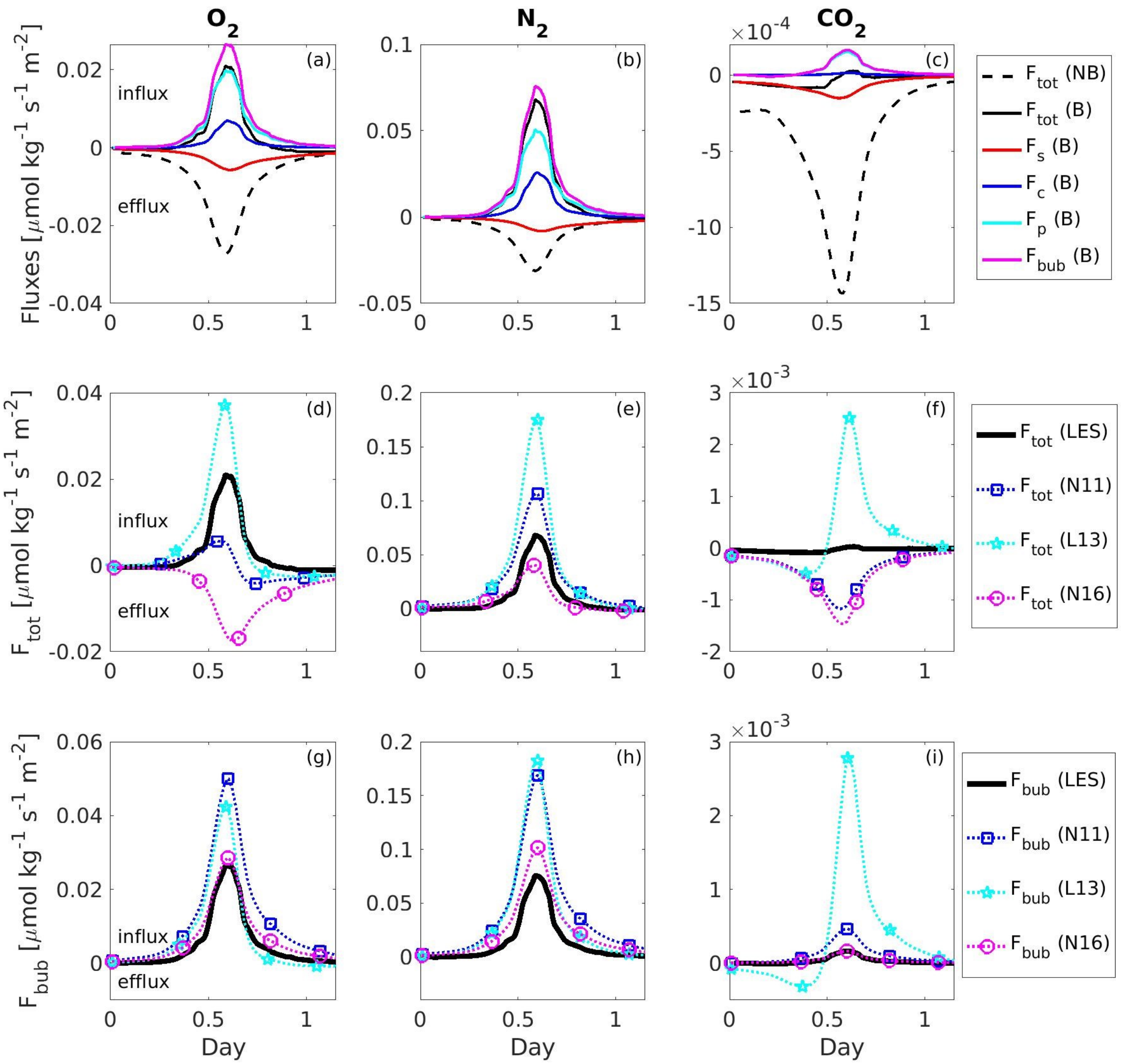

Figure 4. Upper row: The evolution of gas fluxes for total gas flux (F_{tot}), surface gas flux (F_s), gas flux through completely dissolved bubbles (F_c), gas flux through partially dissolved bubbles (F_p), and $F_{bub}=F_c+F_p$ in simulation without bubbles (Run NB) and with bubbles (Run B). Middle row: The comparison of F_{tot} between three parameterizations (N11: *Nicholson et al.* 2011; L13: *Liang et al.* 2013; N16: *Nicholson et al.* 2016) and LES solutions. Lower row: The comparison of F_{bub} between the three parameterizations and LES solutions. The left, middle and right columns are for O_2, N_2, and CO_2, respectively. Positive means influx and negative indicates efflux.